International Journal of Mechanics and Applications 2012, 2(6): 129-139
DOI: 10.5923/j.mechanics.20120206.05

Fluid-Structure Interaction in a Stirred Vessel Equipped with a Rushton Turbine

S. Karray, Z. Driss*, A. Kaffel, H. Kchaou, M. S. Abid

National Engineering School of Sfax (ENIS), Laboratory of Electro-Mechanic Systems (LASEM), University of Sfax, B.P. 1173, km 3.5 Road Soukra, 3038, Sfax, Tunisia

Abstract In this paper, a problem of fluid-structure interaction in a mixing vessel equipped with a Rushton turbine is solved with partitioned coupled fluid-structure interaction computational analysis. The computational fluid dynamics (CFD) code, based on the finite volume method, is used for determination of the flow field in the mixing vessel. The results in form of pressure distribution are then applied to the blade model, which is then analyzed with the computational structure dynamics (CSD) code, based on the finite element method. The resulting displacement is evaluated. The proposed procedure can be effectively used for optimization of structures with significant fluid flow influences. The comparison of the velocity profile with the results founded in the literature shows a good comparison. This proves the validity of the numerical method.

Keywords Computational Fluid Dynamics (CFD), Computational Structure Dynamics (CSD), Fluid-Structure Interaction (FSI), Coupling Algorithm, Rushton Turbine, Turbulent Flow

1. Introduction

The mutual interaction between a fluid flow and a deforming structure is referred to fluid–structure interaction (FSI). Life saving examples are the opening of a parachute [1] or an air bag[2]. Undesired occurrences of fluid–structure interaction are collapses of bridges[3] and cooling towers due to wind and also flutter of aircraft wings[4] and turbine blades[5]. In the biomedical field, the interaction between an elastic artery[6,7] or a heart chamber[8] and the blood that flows through them is of interest. Also for the design of artificial heart valves[9,10], fluid–structure interaction needs to be taken into account. Though efficient solvers for both the fluid and the structural dynamics exist, the development of tools for modeling various FSI problems remains a challenge. As was already mentioned and in order to describe these problems, an exchange of data has to take place between the fluid and structural fields. Based on this data exchange, the methods for solving fluid-structure interaction problems can be divided into monolithic[11-13], and partitioned couplings[14-16]. The first consists on solving both parts of fluid and structure in the same system of equations. The choice of time step is only limited by the required precision. However, this type of algorithm requires a development of a computer code. Moreover, the numerical methods employed for the fluid and the structure domains are different and are difficult to place within the same code, hence the utility of the partitioned algorithm methodology. In the partitioned method, the fluid and structural parts are solved separately. The main advantage of this method is that it allows already developing efficient and well validated solvers for both the fluid and structure subtasks to be combined. Some theoretical and numerical studies of partitioned coupling algorithms for one and two dimensional problems can be found[17]. Particularly, commercial codes for combining existing solvers have been developed. This method has been introduced by Park and Felippa[18], and further investigated by Wood[19]. Various experimental and numerical simulations study the fluid behavior, when the movement of the structure is prescribed analytically [20-22]. Other researchers concentrated on the fluid part, while a simple structural model for a rigid body was used[13]. Further simplifications have been done by neglecting the dynamic effects and simulating static FSI. For example, Beckert et al.[24] used a multivariate interpolation scheme for coupling fluid and structural models in three dimensional spaces. They applied it to static aeroelastic problems, in order to predict the equilibrium of elastic wing models in transonic fluid flow. Seiber[25] developed an efficient coupling algorithm combining FASTEST-3D code and FEAP code for solving various fluid-structure interaction problems in three-dimensional domains for arbitrary elastic structures. Glück et al.[26] applied a partitioned coupling between the CFD code FASTEST-3D and the CSD code ASE to thin shells and membranous structures with large displacements. Bucchig nani et al.[27] presented a numerical code to study the problem of an incompressible flow in a stirred vessel. It was based on a method of a partition treatment type, with the fluid and structural fields resolved

* Corresponding author:
zied.driss@enis.rnu.tn (Z. Driss)
Published online at http://journal.sapub.org/mechanics

by coupling two distinct models. Wang[28] provided an effective new idea to solve aeroelasticity problems, in which the tools Fluent and ABAQUS/ANSYS are employed. Ghavanloo et al.[29] present a simple analytical approach for stationary interaction between the fluid and the cylindrical membrane. They explain the effect of the equilibrium membrane forms elasticity on fluid system. Dang et al.[30] used a coupling algorithm to study the stationary behaviour of a flexible aircraft wing. The finite element method is used for the discretization of the two areas of the structure and fluid.

In this paper, a computational analysis of the fluid-structure interaction in a mixing vessel is presented. In mixing vessels, the fluid can have a significant influence on the deformation blades of during mixing, depending on turbine speed and fluid viscosity. For this purpose, a coupling algorithm has been performed to determine the fluid influences on the Rushton turbine. The fluid field in the mixing vessel was first analyzed with the computational fluid dynamics (CFD) code. The results in the form of pressure were then applied to the blade model, which was the analyzed with the computational structure dynamics (CSD) code. The content of this paper is organized as follows: Section 2 describes the geometry of the system. Section 3 describes the coupling algorithm. Section 4 presents the numerical results. Section 5 contains concluding remarks.

2. Stirred Vessels Configuration

The system was made of a flat bottom cylindrical vessel of diameter D=293 mm, and the liquid height in the vessel was H=D. A Rushton turbine of thickness e=1 mm was attached on the inside wall of the cylindrical tank. It has two arms of diameter d=0.33 D (Figure 1).

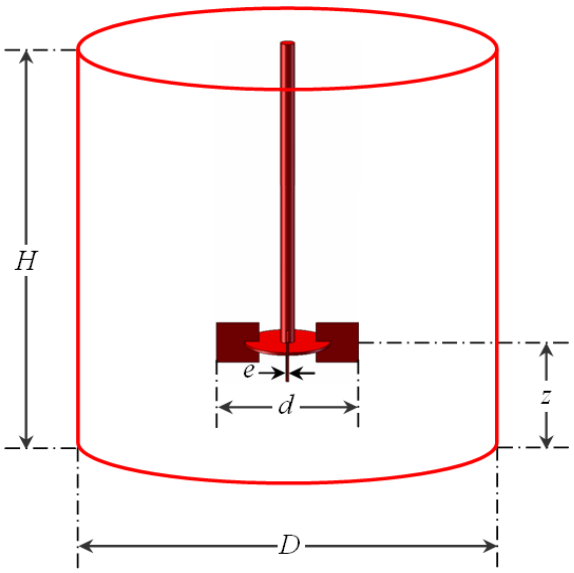

Figure 1. Stirred vessel equipped with Rushton turbine

The clearance between the bottom of the mixing vessel and the blade tip was z=0.33 D. The turbine rotated in a clockwise direction when viewed from above. The origin of the coordinate system used is located in the bottom of the vessel. The geometry of the system resembles the one already experimentally studied by Rushton[31]. In the following investigations, the fluid used in the CFD simulation is the water defined by the density and the viscosity equal respectively to ρ=1000 Kg/m3 and μ=1 mPs. The flow is fully turbulent, where the Reynolds number and the Froude number are equal respectively to Re=104 and Fr=0.02. The structure is assumed to be isotropic linear and elastic material law is applied. Its mechanical characteristics are defined by a Young modulus equal to E=210 MPa, a Poisson's ratio equal to ν=0.28 and a yield stress equal to σ=215 MPa.

3. Coupling Algorithm

In order to make a computational simulation for the fluid-structure interaction phenomena, we used a coupling algorithm to deal with problems of strongly non-linear FSI[32-33]. This algorithm is based on a partitioned method. This method determines the structural and flow solution vectors independently from each other, updating afterwards the relevant boundary conditions. This algorithm requires a CSD code, a CFD code and a coupling interface.

3.1. CFD code

The CFD code allows the hydrodynamic calculation of the fluid[34-37]. The finite volumes method is adopted for the treatment of these equations. Initially, the fluid field is being divided into elementary volumes representing the geometry of the problem. Secondly, the differential equations are discretized using the control volume approach[38]. Several quantities can be found such as the velocity field, pressure, turbulent kinetic energy and its dissipation rate. In a fluid flow problem, we need to know the pressure value at the level of the fluid structure interface. Also, this code must be able to receive information representing displacement of the structure part to be used to solve the fluid flow problem.

3.2. CSD code

The CSD code allows the static calculation of the structure. More precisely, this code must be able to receive information representing the varying physical forces in time exerted by the fluid on the fluid-structure interface. On the other hand, this code is used to determine the displacement of the nodes.

3.3. Coupling Interface

The coupling interface ensures the transfer of the forces and displacements mentioned above, when the mesh in each fluid and structure codes is different. It organizes the transfer of information in time and makes an effective coupling between the fluid and structure codes. For every iteration, the force exerted by the fluid is calculated in the CFD code. The geometry is updated at the interface to calculate the structural displacement by the CSD code. Therefore, the role

of the coupling algorithm is to exchange nearly any kind of data between the coupled codes. The iteration steps are stopped when the convergence is reached. The coupling algorithm was used to study a Rushton turbine in a vessel tank.

4. Numerical Results

4.1. CFD Results

Following the implementation of the CFD code developed in our laboratory LASEM[39], we present the hydrodynamic results such as the velocity field and the turbulence characteristics.

4.1.1. Flow Patterns

Figure 2 shows a velocity vector plot (U,V) in the r-θ plane for six iterations of the coupling algorithm defined by the axial position equal to z=0.66. These results confirm that the velocity field is very high in magnitude on the level of the field swept by the turbine blades. Also, it's noted a predominance of a tangential flow due to the setting in rotation of the volume of the fluid located between blades. Far from the turbine, it's noted a progressive deceleration of the flow. Moreover, the turbine undergoes a deformation due to the flexion of the blade. For thus, the velocity field changes slightly from iteration to another. In fact, after certain iterations ($n_i > 4$), the turbine becomes deformed, and the velocity field is preserved (Figure 2.d).

Figure 3 shows the secondary flow (U,W) in the r-z plane defined by the angular coordinates equal to θ=45°. This presentation plane thought the right blade in an initial state undeformed. The velocity fields show the presence of a radial jet on the level of the turbine. This jet changes against the walls of the tank with two axial flows thus forming two recirculation zones on both sides of the turbine. In addition, we observe that the axial jet is more intense during the first iteration. From iteration to another, the axial jet weakens. This fact generates an increase of the dead zone in the tank top. Indeed, the position of the circulation zone approaches towards the turbine axis. This phenomenon is completely logical since the position of the various planes representation during the iterations was deviated compared to the blade of the turbine which behaves like a curved blade turbine after deformation. By comparing the various iterations between them, it's noted a weak variation of the velocity field starting from the second iteration.

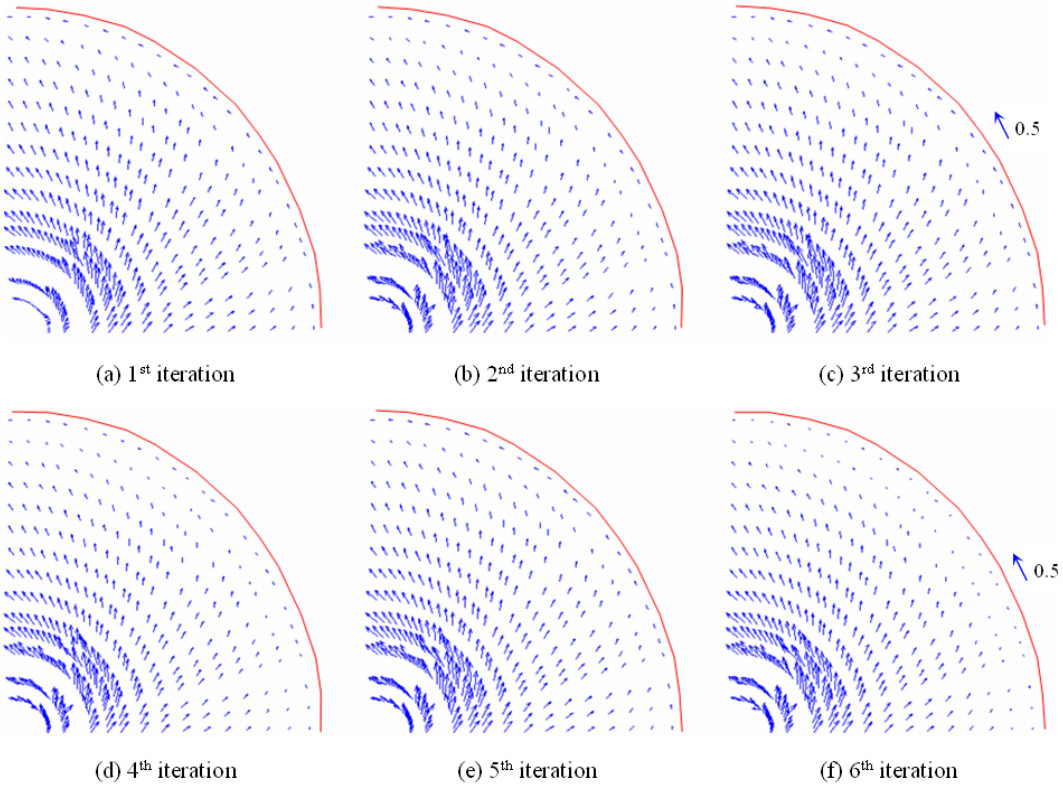

Figure 2. Flow patterns induced in the r-θ plane defined by z=0.66

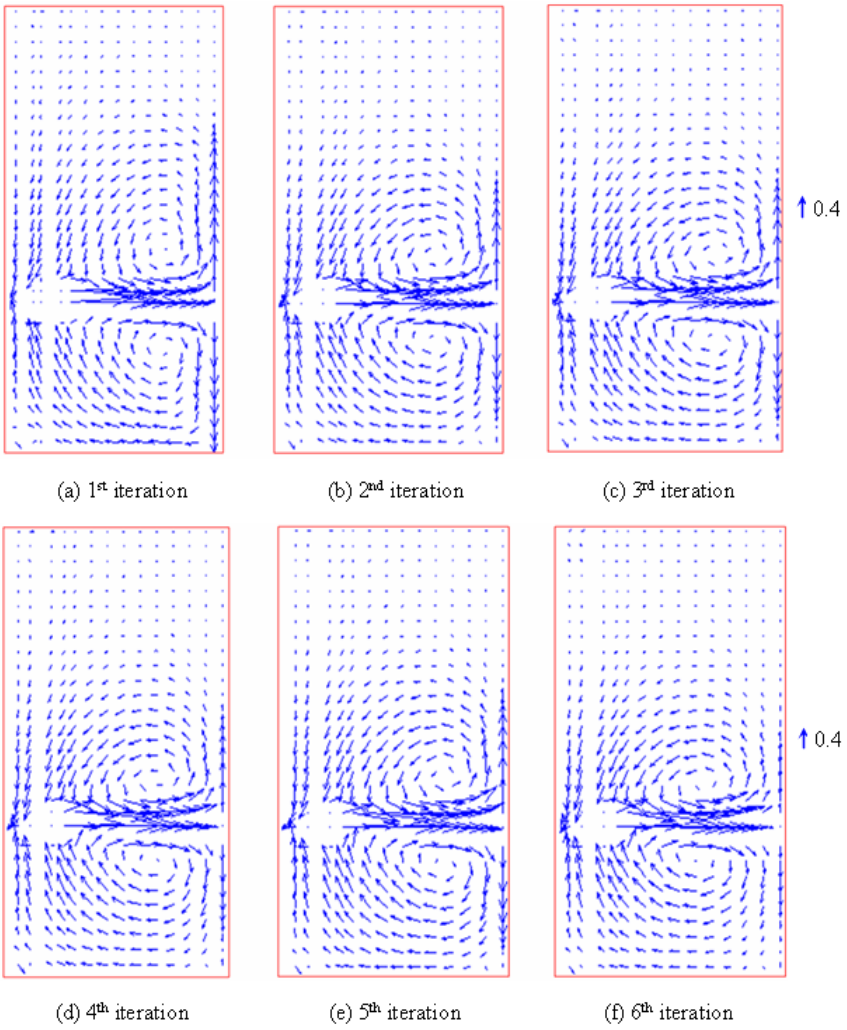

Figure 3. Flow patterns induced in the *r*-*z* plane defined by θ=45°

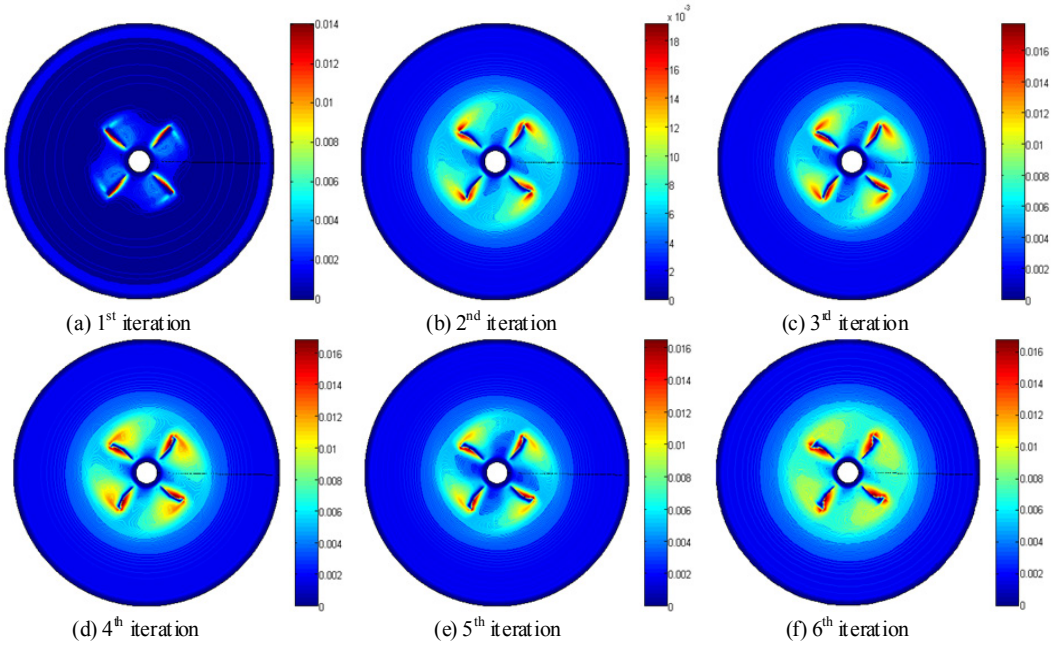

Figure 4. Distribution of the turbulent kinetic energy in *r*-θ plane

4.1.2. Distribution of the Turbulent Kinetic Energy

Figure 4 presents the evolution of the distribution of the turbulent kinetic energy k in the horizontal plane defined by the axial position equal to z=0.66. Figure 5 presents the distribution of the turbulent kinetic energy k in the r-z plane during the six iterations of the coupling algorithm. This plane is located at the level of the turbine blade and defined by the angular position equal to θ=45°. According to these results, it's noted that the maximum values are located in the wake developed upstream of the turbine blade. In the field swept by the turbine blade, the turbulent kinetic energy remains rather high. Outside this domain, the turbulent kinetic energy quickly becomes very low. By comparing these results from iteration to another, we observe that the maximal values are reached during the second iteration and it's equal to k=0.018.

4.1.3. Distribution of Dissipation Rate of the Turbulent Kinetic Energy

Figure 6 shows the distribution of the dissipation rate of the turbulent kinetic energy ε in the horizontal plane during the six iterations of the coupling algorithm. This plane correspond to an axial position defined by z=0.66. Figure 7 shows the distribution of the dissipation rate of the turbulent kinetic energy ε in the r-z plane for an angular position equal to θ=45° during the first six iterations of the algorithm of coupling. Globally, we observe a distribution similar to that already obtained with the turbulent kinetic energy. Indeed, it's noted that the maximal values are located near the blade end. However, the rate of wake becomes very weak outside the domain swept by the turbine blades. The maximal value of the dissipation rate of the turbulent kinetic energy is reached in the sixth iteration and it is equal to ε=0.032.

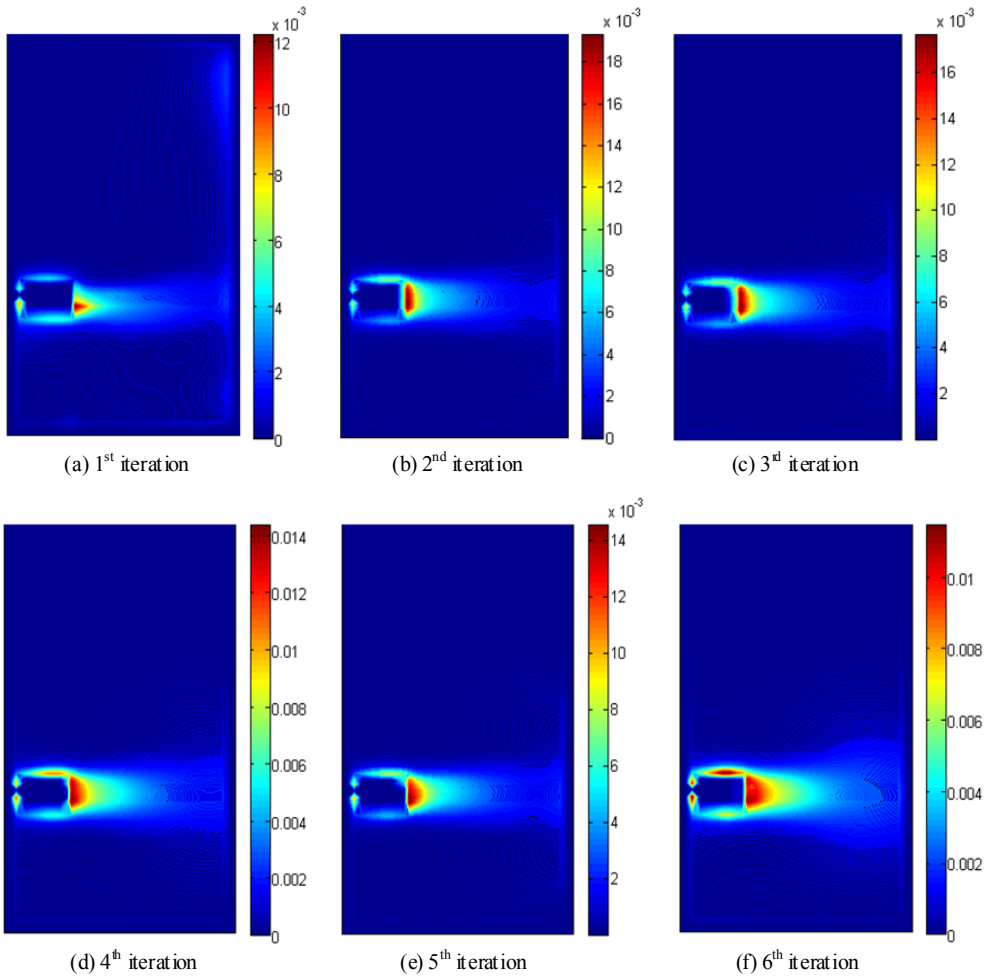

(a) 1st iteration (b) 2nd iteration (c) 3rd iteration

(d) 4th iteration (e) 5th iteration (f) 6th iteration

Figure 5. Distribution of the turbulent kinetic energy in r-z plane

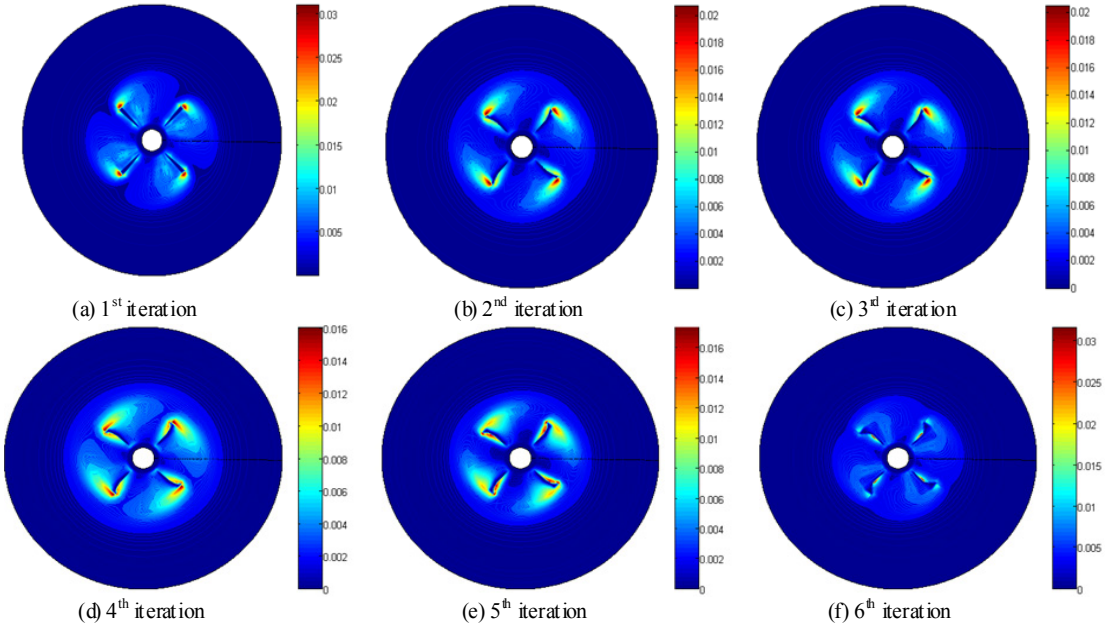

(a) 1st iteration (b) 2nd iteration (c) 3rd iteration

(d) 4th iteration (e) 5th iteration (f) 6th iteration

Figure 6. Dissipation rate of the turbulent kinetic energy ε in the r-θ plane defined by z=1

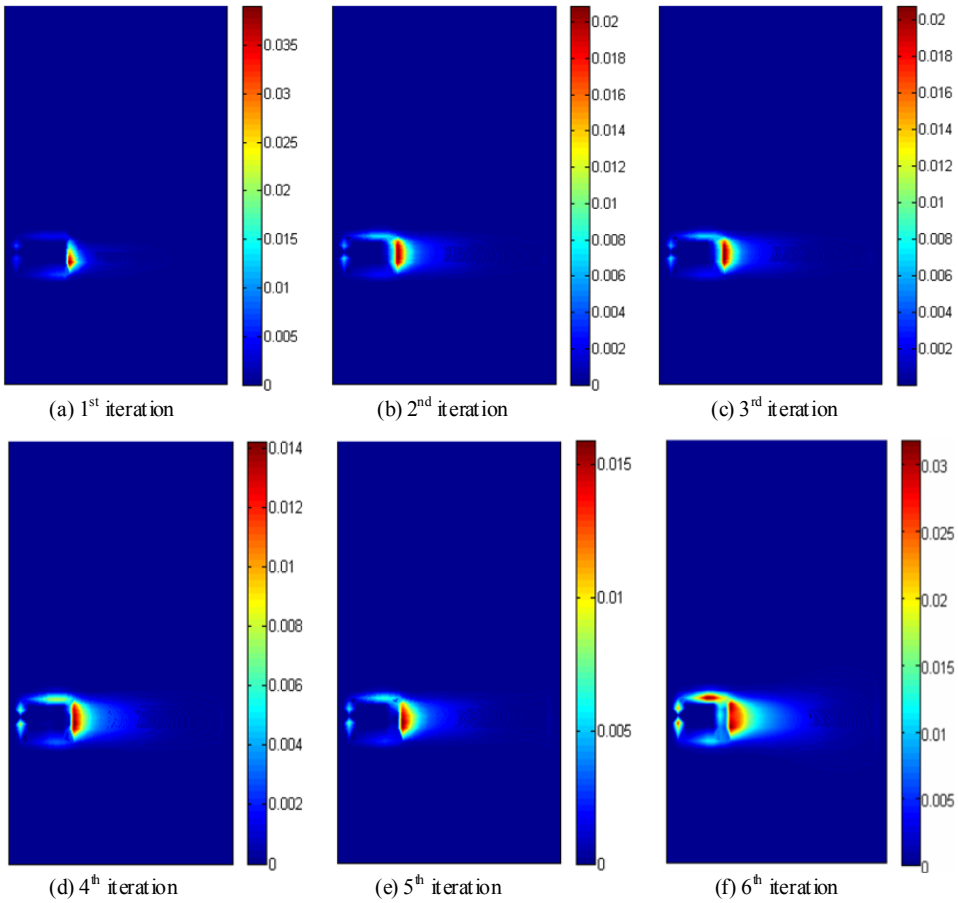

(a) 1st iteration (b) 2nd iteration (c) 3rd iteration

(d) 4th iteration (e) 5th iteration (f) 6th iteration

Figure 7. Dissipation rate of the turbulent kinetic energy ε in the r-z plane defined by θ=45°

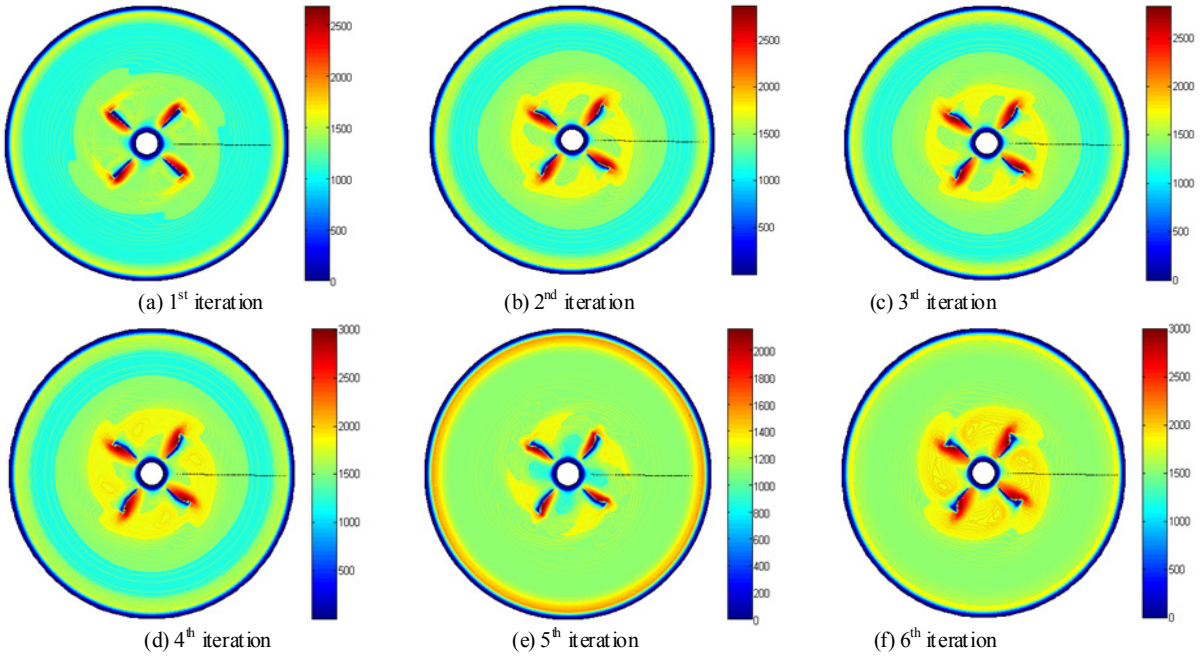

Figure 8. Turbulent viscosity in the r-θ plane defined by z=0.16

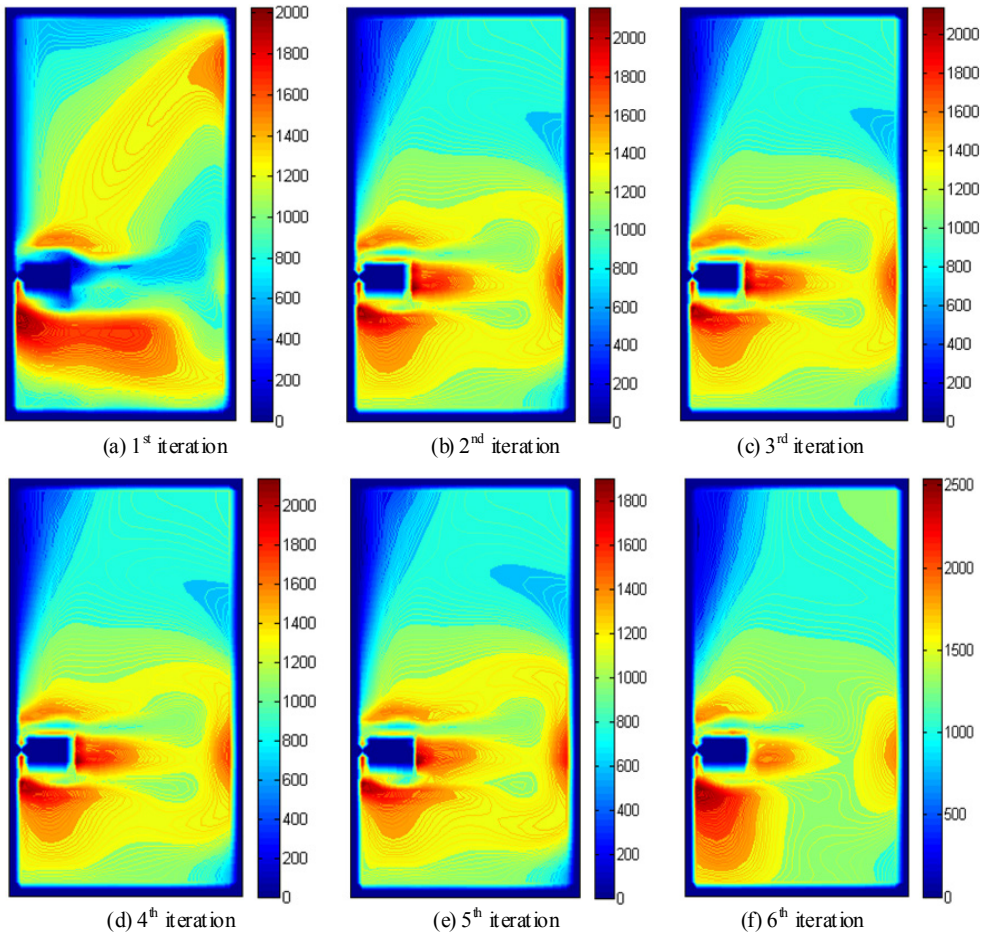

Figure 9. Turbulent viscosity in the r-z plane defined by θ=45°

4.1.4. Distribution of the Turbulent Viscosity

Figure 8 shows the evolution of the distribution of the turbulent viscosity in the horizontal plane located in the bottom of the turbine during the iterations of the coupling algorithm. The presentation plane corresponds to the axial position equal to z=0.66. Figure 9 presents the distribution of the turbulent viscosity in the vertical plane defined by the

angular position equal to θ=45°. It corresponds to the plane located at the level of the turbine blade. In these conditions, the vertical arm deformation reaches the representation plane. This is visualized by the presence of a zone where the turbulent viscosity of the fluid is null. This zone corresponds to the blade of the Rushton turbine in the initial state (Figure 9.a). Then, it decreases from iteration to another. Also, we find that the maximum value of the turbulent viscosity is obtained during the sixth iteration and is equal to υ_t=2500 (Figure 9.c). Indeed, it's noted that the turbulent viscosity remains rather high in the field swept by the turbine blade. However, the turbulent viscosity quickly decreases near the walls. This phenomenon is due to the slowing down of the flow.

4.1.5. Comparison with Anterior Results

Figure 10 presents the radial profiles of the dimensionless angular velocity component V(r). The axial coordinate is equal to z=0.7. In this figure, the results found by Alcamo et al.[40] are superposed. The error is equal to 9%. The good agreement between the results confirms the validity of the numerical method.

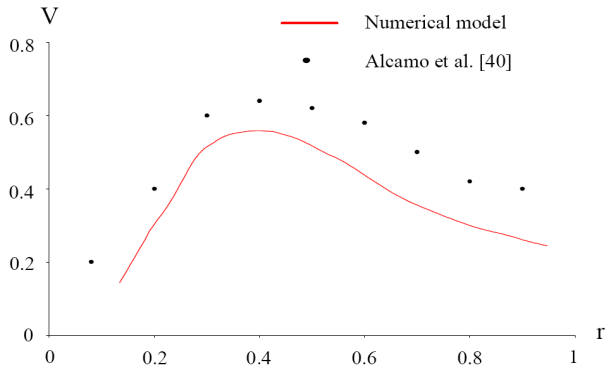

Figure 10. Radial profiles of the angular velocity V(r)

4.2. Static Studies

In the static studies, we are interested in the structural part of the mixing system. Particularly, the static behavior of the Rushton turbine and the deformation of the blade under the flow effect have been studied. The discretisation is ensured by finite elements method. In these conditions, 2411 tetrahedral type nodes defined on the axis and the disc of the turbine. However, 245 quadratic type nodes arevdefined on etch blade (Figure 11). Figure 12 presents the results from the CSD code to study the static behaviour of the Rushton turbine and the evolution of the displacement field of the blade during various iterations of our coupling algorithm. Particularly, we are interested in the nodal displacement of the turbine blade to mesh the fluid domain. This operation is repeated several times until equilibrium is obtained. According to these results, it's noted that the maximal displacement is obtained in the first iteration.

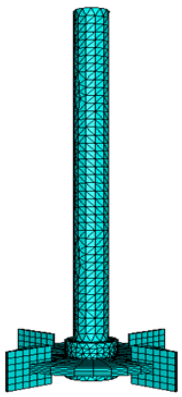

Figure 11. Meshing

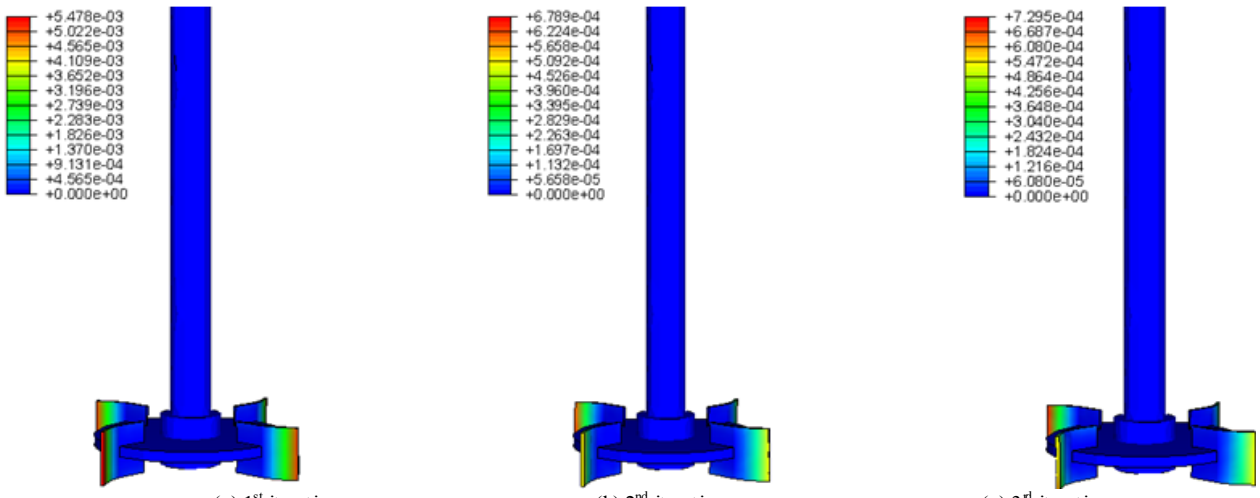

(a) 1st iteration (b) 2nd iteration (c) 3rd iteration

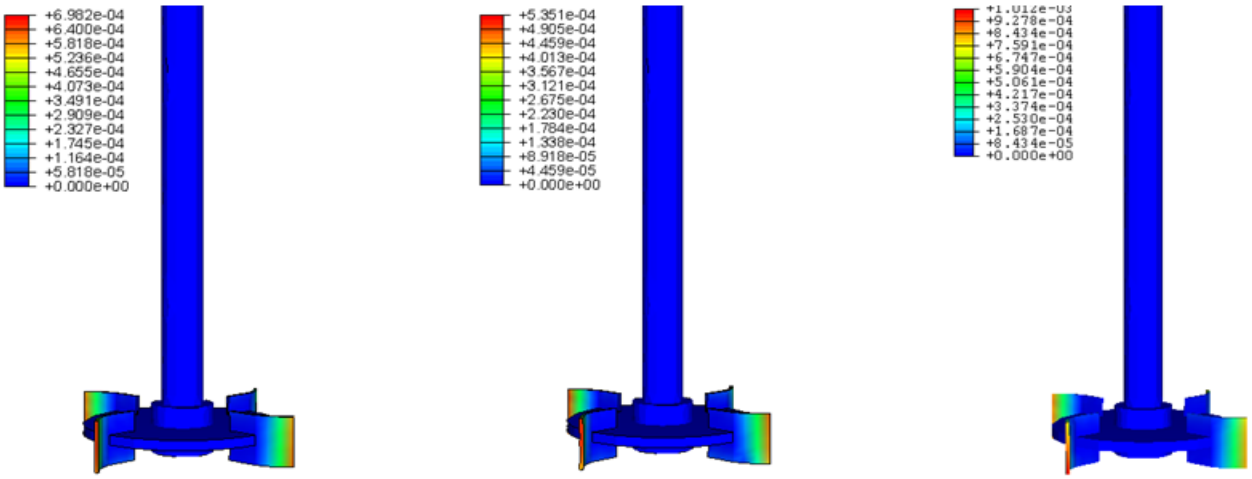

(d) 4th iteration (e) 5th iteration (f) 6th iteration

Figure 12. Displacement field of the turbine Rushton

5. Conclusions

In this paper, coupling codes are used for solving fluid-structure interaction (FSI) problems in the stirred tank equipped by a Rushton turbine. A computational fluid dynamics (CFD) code and a computational structural dynamics (CSD) code have been coupled by using an efficient coupling interface. Particularly, the fluid field in stirred tank was solved by the CFD code in turbulent regime. The deformation of the Rushton turbine was solved by the CSD code. Specific techniques of rearrangement of grid and treatment of the boundary conditions are used to follow the behaviour of the system. This method takes advantage of the parallel process involved with each analysis code. This allows both parts of the fluid-structure interaction problem to be solved in the best possible way: a Finite Volume Method for the fluid dynamics and a Finite Element Method for the structure. The CFD results obtained allow a visualizing of the velocity field, the turbulent kinetic energy, the dissipation rate of the turbulent kinetic energy, the turbulent viscosity and the mechanical deformation. These results proof that the fluid flow have a significant effect on the deformation of the Rushton turbine blade. For thus, it's fundamental to take consideration of this phenomenon in the design of the industrial process.

NOMENCLATURE

d turbine diameter, m
z Height of the blade, m
e Thickness of the blade, m
D Internal diameter of the vessel tank, m
Fr Froude number, dimensionless
z turbine position, m
H vessel tank height, m
k turbulent kinetic energy, dimensionless
Re Reynolds number, dimensionless,
r radial coordinate, dimensionless
s shaft diameter, m
U radial velocity components, dimensionless
V angular velocity components, dimensionless
W axial velocity components, dimensionless
z axial coordinate, dimensionless
n_i iteration number
υ_t turbulent viscosity

REFERENCES

[1] Tezduyar, T., Sathe, S., and Stein, K., 2006, Solution techniques for the fully discretized equations in computation of fluid–structure interactions with the space-time formulations, Computer Methods in Applied Mechanics and Engineering, 195 (41-43), 5743-5753.

[2] Khan, M., Moatamedi, M., Souli, M., and T. Zeguer, 2008, Multiphysics out of position airbag simulation, International Journal of Crashworthiness, 13 (2), 159-166.

[3] Billah, K., and Scanlan, R., 1991, Tacoma Narrows Bridge Failure, and Undergraduate Physics Textbooks, American Journal of Physics, 59 (2), 118-124.

[4] Farhat, C., Van der Zee, K., and Geuzaine, P., 2006, Provably second-order time-accurate loosely-coupled solution algorithms for transient nonlinear computational aeroelasticity, Computer Methods in Applied Mechanics and Engineering, 195 (17-18), 1973-2001.

[5] Willcox, K., Paduano, J., Peraire, J., 1999, Low order aerodynamic models for aeroelastic control of turbomachines, in: 40th AIAA/ASME/ASCE/AHS/ASC Structures, Structural Dynamics and Materials Conference, St Louis, MO, USA, 1-11.

[6] Gerbeau, J.-F., Vidrascu, M., Frey, P., 2005, Fluid-structure interaction in blood flows on geometries based on medical imaging, Computers & Structures, 83 (2–3), 155-165.

[7] Wall, W., Rabczuk, T., 2008, Fluid-structure interaction in lower airways of CT-based lung geometries, International Journal for Numerical Methods in Fluids, 57 (5), 653-675.

[8] Peskin, C., 1977, Numerical analysis of blood flow in the heart, Journal of Computational Physics, 25 (3), 220-252.

[9] Peskin, C., 1972, Flow patterns around heart valves: a numerical method, Journal of Computational Physics, 10 (2), 252-271.

[10] Dumont, K., Vierendeels, J., Kaminsky, R., G. Van Nooten, Verdonck, P. Bluestein, D., 2007, Comparison of the hemodynamic and thrombogenic performance of two bileaflet mechanical heart valves using a CFD/FSI model, Journal of Biomechanical Engineering - Transactions of the ASME, 129 (4), 558-565.

[11] Van Brummelen, E.H., Hulshoff, S.J., and De Borst, R., 2003, Energy conservation under incompatibility for fluid-structure interaction problems, Computer Methods in Applied Mechanics and Engineering. 192, 2727-2748.

[12] Michler, C., Hulshoff, S. J., Van Brummelen, E. H., and De Borst, R., 2004, A monolithic approach to fluid-structure interaction, Computers & Fluids, 33, 839-848.

[13] Wick, T., 2012, Goal-oriented mesh adaptivety for fluid-structure interaction with application to heat-valve settings, the Archive of Mechanical Engineering, VOL. LIX, Number 1, 73-99.

[14] Piperno, S., and Farhat, C., 2001, Partitioned procedures for the transient solution of coupled aeroelastic problems - Part II: energy transfer analysis and three-dimensional applications, Computer Methods in Applied Mechanics and Engineering, 190, 3147-3170.

[15] Sternel, D. C., Schäfer, M., Heck, M., and Yigit, S., 2008, Efficiency and accuracy of fluid-structure interaction simulations using an implicit partitioned approach. Comput Mech. 43, 103-113.

[16] Karray, S., Driss, Z., Kchaou, H., Abid, M.S., 2011, Numerical simulation of fluid-structure interaction in a stirred vessel equipped with an anchor impeller, Journal of Mechanical Science and Technology, 25 (7), 1-12.

[17] Cebral, C., Piperno S., and Larrouturou, B., 1995, Partitioned procedures for the transient solution of coupled aeroelastic problems. Part 1: Model problem, theory and two-dimensional application, Journal of Computer Methods in Applied Mechanics and Engineering, 124, 79-112.

[18] Park, K.C., and Felippa, C., 1983, A Partitioned analysis of coupled systems, Computational Methods for Transient Analysis in Computational Methods in Mechanics, 1, 157-218.

[19] Wood, W.M., 1990, Practical Time-stepping Schemes, Oxford University Press, New York.

[20] Pedley, T.J., and Stephanoff, K.D., 1985, Flow along a channel with a time-dependent indentation in one wall: the generation of vorticity waves, Journal of Fluid Mechanics. 160, 337-367.

[21] Ralph, M.E., and Pedley, T.J., 1989, Viscous and inviscid flows in a channel with a moving indentation, Journal of Fluid Mechanics, 209, 543-566.

[22] Natarajan, S., and Mokhtarzadeh-Dehghan, M.R., 2000, Numerical prediction of a (potential) soft acting peristaltic blood pump, International Journal for Numerical Methods in Fluids, 32, 711-724.

[23] Cossu, C., and Morino, L., 2000, On the instability of a spring-mounted circular cylinder in a viscous flow at low Reynolds numbers, Journal of Fluids and Structures, 14, 183-196.

[24] Beckert, A., and Wendland, H., 2001, Multivariate interpolation for fluid-structure interaction problems using radial basis functions, Aerospace, Science and Technology, 5, 125-134.

[25] Sieber, G., 2002, Numerical Simulation of Fluid-Structure Interaction Using Loose Coupling Methods, PhD thesis, at the Department of Numerical Methods in Mechanical Engineering, Darmstadt University of Technology.

[26] Glück, M., Breuer, M., Durst, F., Hlfmann, A., and Rank, E., 2003, Computation of wind-induced vibrations of flexible shells and membranous structures. Journal of Fluids and Structures, 17, 739-765.

[27] Bucchignani, E., Stella F., and Paglia F., 2004, A partition method for the solution of a coupled liquid-structure interaction problem, Applied Numerical Mathematics, 51, 463-475.

[28] Wang, Y., 2008, Combination of CFD and CSD packages for fluid-structure interaction, Journal of Hydrodynamics, 20, 756-761.

[29] Ghavanloo, E., and Farhang, D., 2010, Analytical analysis of the static interaction of fluid and cylindrical membrane structures, European Journal of Mechanics A/Solids 29, 600-610.

[30] Dang, H., Yang, Z. and Li, Y., 2010, Accelerated loosely-coupled CFD/CSD method for nonlinear static aeroelasticity, Analysis Aerospace Science and Technology 14, 250-258

[31] Rushton, J.H., Costich, E.W., Everett, H.J., 1950, Power characteristics of mixing impellers, Chemical Engineering Progress, Vol. 46, 467-476,.

[32] Driss, Z., Karray, S., Kchaou, H., and Abid, M.S., 2007, Computer Simulations of Fluid-Structure Interaction Generated by a Flat-Blade Paddle in a Vessel Tank, International Review of Mechanical Engineering (I.RE.M.E.), 1, 608-617.

[33] Karray, S., Driss, Z., Kchaou, H., Abid, M.S., 2011, Hydromechanics characterization of the turbulent flow generated by anchors impellers. Engineering Applications of Computational Fluid Mechanics, 5 (3), 315-328.

[34] Patankar, S.V., 1980, Numerical heat transfer and fluid flow, Series in Computational Methods in Mechanics and Thermal Sciences, McGraw Hill, New York.

[35] Chtourou, W., Ammar, M., Driss Z., and Abid, M.S., 2011, Effect of the turbulence models on Rushton turbine generated flow in a stirred vessel, Cent. Eur. J. Eng., 1, 380-389.

[36] Ammar, M., Driss, Z., Chtourou, W., and Abid, M.S., 2011, Effects of baffle length on turbulent flows generated in stirred vessels, Cent. Eur. J. Eng., 1, 401-412.

[37] Ammar M., Driss Z., Chtourou W., Abid M.S., 2012, Effect of the Tank Design on the Flow Pattern Generated with a Pitched Blade Turbine, International Journal of Mechanics and Applications, Vol. 2, N. 1, pp. 12-19.

[38] Driss, Z., Karray, S., Kchaou, H., and Abid, M.S., 2011, CFD simulation of the laminar flow in stirred tanks generated by

double helical ribbons and double helical screw ribbons impellers, Cent. Eur. J. Eng., 1, 413-422.

[39] Driss, Z., Bouzgarrou, G., Chtourou, W., Kchaou H., and Abid, M.S., 2010, Computational studies of the pitched blade turbines design effect on the stirred tank flow characteristics, European Journal of Mechanics B/Fluids, 29, 236-245.

[40] Alcamo, R., Micale, G., Grisafi, F., Brucato, A., and Ciofalo, M., 2005, Large-eddy simulation of turbulent an unbaffled stirred tank driven by a Rushton turbine, Chemical Engineering Science, 60, 230 –2316.